

# Irreversible magnetization under rotating fields and lock-in effect on $\text{ErBa}_2\text{Cu}_3\text{O}_{7-\delta}$ single crystal with columnar defects

M. A. Avila<sup>a</sup>, L. Civale<sup>b</sup>, A. V. Silhanek<sup>b</sup>, R. A. Ribeiro<sup>a</sup>, O. F. de Lima<sup>a</sup>, H. Lanza<sup>c</sup>

<sup>a</sup>*Instituto de Física "Gleb Wataghin", UNICAMP, 13083-970, Campinas - SP, Brazil.*

<sup>b</sup>*Comisión Nacional de Energía Atómica - Centro Atómico Bariloche and Instituto Balseiro, 8400 Bariloche, Argentina.*

<sup>c</sup>*Comisión Nacional de Energía Atómica - Departamento de Física, Buenos Aires, Argentina.*

(June 15, 2001)

We have measured the irreversible magnetization ( $\mathbf{M}_i$ ) of an  $\text{ErBa}_2\text{Cu}_3\text{O}_{7-\delta}$  single crystal with columnar defects (CD), using a technique based on sample rotation under a fixed magnetic field  $H$ . This method is valid for samples whose magnetization vector remains perpendicular to the sample surface over a wide angle range - which is the case for platelets and thin films - and presents several advantages over measurements of  $\mathbf{M}_L(H)$  loops at fixed angles. The resulting  $\mathbf{M}_i(\Theta)$  curves for several temperatures show a peak in the CD direction at high fields. At lower fields, a very well defined plateau indicative of the vortex lock-in to the CD develops. The  $H$  dependence of the lock-in angle  $\varphi_L$  follows the  $H^{-1}$  theoretical prediction, while the temperature dependence is in agreement with entropic smearing effects corresponding to short range vortex-defects interactions.

## I. INTRODUCTION

The study of the angular dependence of vortex pinning in high temperature superconductors (HTSC) with tilted columnar defects has revealed a richer variety of phenomena and pinning regimes than originally expected. At high temperatures and magnetic fields, the uniaxial nature of pinning by CD dominates the vortex response<sup>1</sup>. This is clearly seen, for instance, when isothermal magnetization loops  $\mathbf{M}(\mathbf{H})$  are measured for different field orientations<sup>2</sup>. At fixed field modulus  $H$ , the irreversible magnetization  $M_i = \frac{1}{2}\Delta M$  (where  $\Delta M$  is the width of the hysteresis, proportional to the persistent current density  $J$ ) exhibits a well defined maximum when  $\mathbf{H} \parallel \text{CD}$ . For other orientations "staircase vortices" develop. In a previous study we have shown<sup>2</sup> that in  $\text{YBa}_2\text{Cu}_3\text{O}_7$  (YBCO), and due to the simultaneous presence of CD, twin boundaries and crystallographic ab-planes, correlated pinning dominates over random pinning for all orientations, forming staircases of different configuration (i.e., with segments locked into different correlated structures) depending on the field direction.

An additional feature is the existence of a lock-in phase. When the angle between  $\mathbf{H}$  and the CD is less than a lock-in angle  $\varphi_L(H, T)$ , it is energetically convenient for vortices to ignore the  $\mathbf{H}$  orientation and to remain locked into the tracks<sup>3,4</sup>. Since  $\varphi_L$  scales as  $1/H$ , in practice this effect is only visible at low fields. An experimental manifestation of the lock-in regime is the existence<sup>2</sup> of a "plateau" in the irreversible magnetization,  $M_i(\Theta) \approx \text{const}$ , over a certain angular range. Here  $\Theta$  is the angle between the normal to the platelet crystal,  $\mathbf{n}$  (which coincides with the crystallographic c-axis) and  $\mathbf{H}$ , defined within the plane that contains the CD.

At low fields, an additional effect must be taken into account. Due to both the anisotropic superconducting response of the HTSC and the sample geometry, the di-

rection of the internal field  $\mathbf{B}$ , that coincides with the direction of the vortices, differs from that of  $\mathbf{H}$ . As the uniaxial pinning of the CD maximizes when  $\mathbf{B}$  (rather than  $\mathbf{H}$ ) is aligned with the tracks, the maximum in  $M_i(\Theta)$  occurs at an angle that progressively departs<sup>2</sup> from the orientation of the tracks,  $\Theta_D$ , as  $H$  decreases.

The low field misorientation between  $\mathbf{B}$  and  $\mathbf{H}$  poses a serious experimental concern. All studies of the pinning properties of tilted CD that are based solely on measurements at  $\mathbf{H} \parallel \text{CD}$ , or on comparison of this orientation with a few others, give valid information at high fields, but are misleading at low fields; vortices are just not oriented in the right direction. To avoid this problem, a rather complete knowledge of the angular dependent response,  $M_i(H, \Theta)$ , is required.

In this work we present a procedure that allows us to obtain directly  $M_i(\Theta)$  by rotating the sample at fixed  $H$  and  $T$ . This method has the advantage that a fine grid can be easily obtained in the angular ranges of interest, thus permitting the exploration of the various regimes with significantly improved angular resolution. We apply this experimental procedure to investigate the pinning produced by tilted CD in an  $\text{ErBa}_2\text{Cu}_3\text{O}_7$  single crystal. We present a detailed analysis of the lock-in angle as a function of  $H$  and  $T$ . The width of the lock-in regime is shown to follow a  $1/H$  dependence over a wide temperature range, and from the temperature dependence of the slope of  $\varphi_L$  vs  $1/H$  we determine the entropic smearing function  $f(T/T^*)$ .

## II. EXPERIMENTAL DETAILS

The sample used in this work is a rectangular  $\text{ErBa}_2\text{Cu}_3\text{O}_{7-\delta}$  single crystal platelet of dimensions  $0.44 \times 0.33 \times 0.01 \text{ mm}^3$ , grown by the self-flux method in a commercial yttria-stabilized-zirconia crucible<sup>6</sup>. After

growth it was annealed under oxygen atmosphere for 7 days at 450°C. This sample was then irradiated with 309 MeV  $Au^{26+}$  ions (whose penetration range in this material is  $\sim 15\mu m$ ) at the TANDAR accelerator in Buenos Aires (Argentina), to introduce columnar defects at an angle  $\Theta_D \approx 30^\circ$  off the  $c$  axis. The rotation axis, which is perpendicular to the plane formed by the  $c$ -axis and the track's direction, is parallel to the largest crystal dimension. The irradiation dose was equivalent to a matching field of  $B_\Phi = 1T$ . After irradiation the sample presented a superconducting transition temperature of  $T_c = 90.0K$  and transition width of  $\Delta T < 1K$ .

Magnetization experiments were conducted on a commercial superconducting quantum interference device (SQUID) magnetometer (Quantum Design MPMS-5), equipped with two sets of detectors that allow to record both the longitudinal ( $M_L$ ) and transverse ( $M_T$ ) components of the magnetization vector  $\mathbf{M}$ , with respect to the longitudinally applied field  $\mathbf{H}$ . We have developed a sample rotation system (hardware and software) that solves the problems usually involved in the measurement of  $M_T$ , and thus allows us to study the response of the samples at arbitrary orientations. We have used that system in the past to measure magnetization loops  $\mathbf{M}(\mathbf{H})$  at different field orientations in samples similar to the one investigated here.<sup>2,5</sup> In those experiments the sample is initially rotated to the desired  $\Theta$ , then zero-field-cooled (ZFC) from above  $T_c$  to the desired measuring temperature  $T$ . Both  $M_L(H)$  and  $M_T(H)$  are then measured, and the separation between the upper and lower branches of both loops ( $\Delta M_L(H)$  and  $\Delta M_T(H)$ ) is used to calculate the amplitude  $M_i = \frac{1}{2}\sqrt{\Delta M_L(H)^2 + \Delta M_T(H)^2}$  and direction  $\Theta_M = \arctan(\Delta M_T(H)/\Delta M_L(H))$  of the irreversible magnetization vector  $\mathbf{M}_i$ .

The alternative rotating sample measurements presented here are performed by setting up a desired initial state ( $T, H, \Theta_H$ ) and then recording  $M_L(\Theta)$  and  $M_T(\Theta)$  for fixed  $T$  and  $H$ . The sample is rotated a given angle step (typically  $1^\circ$  to  $3^\circ$ ) and re-measured. Usually, the procedure is repeated until the crystal completes 2 or 3 full turns. This provides us with redundant information that contributes to improve the quality of the data. After careful subtraction of the signal of the plastic sample holder (which has only longitudinal component and is small, linear in  $H$ , almost temperature independent and, most importantly, angle independent) and of the reversible response, the irreversible components  $M_{Li}(H)$  and  $M_{Ti}(H)$  are used to determine  $M_i = \sqrt{M_{Li}(H)^2 + M_{Ti}(H)^2}$  and  $\Theta_M = \arctan(M_{Ti}(H)/M_{Li}(H))$ .

### III. ROTATING MEASUREMENTS

#### A. Meissner response

We began this study with an analysis of the Meissner response. To that end we ZFC the crystal, then applied a field  $H$  smaller than the lower critical field  $H_{c1}(\Theta)$  for all  $\Theta$ , and subsequently performed the rotating measurements. Ideally, under those conditions there are no vortices in the crystal and the response depends neither on the material anisotropy nor on the pinning properties, it is totally determined by the sample geometry. As was previously shown<sup>7</sup>,  $M_L(\Theta)$  and  $M_T(\Theta)$  for a thin platelet should follow the dependencies

$$4\pi M_L(\Theta) = -H \left( \frac{1}{2\nu} \cos^2 \Theta + \frac{1}{1-\nu} \sin^2 \Theta \right) \quad (1)$$

$$4\pi M_T(\Theta) = -H \left( \frac{1}{2\nu} - \frac{1}{1-\nu} \right) \sin \Theta \cos \Theta \quad (2)$$

where  $\nu$  is the appropriate demagnetizing factor, which is essentially given by the thickness of the platelet ( $t$ ) divided by its width ( $W$ ). These equations can be easily rewritten as

$$M_L = -M_0 - M_{2\Theta} \cos 2\Theta_H \quad (3)$$

$$M_T = -M_{2\Theta} \sin 2\Theta_H \quad (4)$$

where

$$4\pi M_0 = \frac{H}{2} \left( \frac{1}{2\nu} + \frac{1}{1-\nu} \right) \quad (5)$$

$$4\pi M_{2\Theta} = \frac{H}{2} \left( \frac{1}{2\nu} - \frac{1}{1-\nu} \right) \quad (6)$$

Equations 3 and 4 indicate that the magnetization vector  $\mathbf{M}$  can be visualized as the sum of a fixed contribution  $\mathbf{M}_0$ , anti-parallel to  $\mathbf{H}$ , and a rotating contribution  $\mathbf{M}_{2\Theta}$  with a periodicity of  $180^\circ$ . This suggests that a convenient way to plot these data is on an  $M_L, M_T$  plane. In this presentation the Meissner response is expected to lie on a circumference of radius  $M_{2\Theta}$  centered at  $(M_L, M_T) = (-M_0, 0)$ . One complete circumference is drawn by a rotation of  $180^\circ$ . An example of this procedure (for  $T = 60K$  and  $H = 50Oe$ ) is shown in Figure 1. The crystal was rotated by two complete turns, thus there are four sets of data points covering  $180^\circ$  each, which are clearly separated in two groups. This is due to a small remnant magnetization  $\mathbf{M}_R$ , which originates from the small residual field that is usually present during the ZFC.<sup>7</sup>

The vector  $\mathbf{M}_R$  has fixed modulus and its direction remains fixed with respect to the sample during rotation,<sup>7</sup> thus  $M_{RL} = M_R \cos(\Theta + \Theta_R)$  and  $M_{RT} = M_R \sin(\Theta + \Theta_R)$ , where  $M_R$  and  $\Theta_R$  are constants.

Since  $\mathbf{M}_R(\Theta)$  has a one fold periodicity, it breaks the Meissner two fold periodicity and splits the experimental data into two sets. Indeed, by fitting the data in Fig. 1 using a combination of the Meissner and remnant contributions we can easily determine and remove the remnant part and all points collapse on a single circumference (solid symbols). Fig. 1 is an extreme example of remnant influence, chosen to show that even in that case the Meissner response can be obtained. By carefully canceling the residual magnetic field in the ZFC procedure we can obtain a much smaller  $\mathbf{M}_R$  such that both circumferences of raw data in Fig. 1 almost collapse on a single one.

Equations 3 and 4 were used to fit several measurements for different temperatures and fields, and used to calculate the sample volume  $V \approx 1.45 \times 10^{-6} \text{cm}^3$  and demagnetization factor  $\nu \approx 0.033$ . Both results are in very good agreement with the values directly determined from crystal dimensions ( $V \sim 1.46 \times 10^{-3} \text{cm}^3$ ;  $\nu \approx 0.03$ ).

### B. critical state

We now focus on the high field range, where the crystal is in the mixed state. Fig. 2(a) shows  $M_L(\Theta)$  and  $M_T(\Theta)$  for a rotation at 70K and 8kOe, where the angle independent background due to the holder has already been removed from  $M_L$ . As the reversible magnetization of the superconductor [ $\sim (\Phi_0/32\pi^2\lambda^2) \ln(H_{c2}/H) \sim 5G$ ] is negligible compared to  $\mathbf{M}_i$ , the response is dominated by vortex pinning. Curves in Fig. 2(a) exhibit a rich structure, due to the combination of crystalline anisotropy, directional vortex pinning and geometrical effects. In order to extract useful information from them, we must first establish the relation between  $\mathbf{M}_i$  and the screening current  $\mathbf{J}$  flowing through the crystal.

For simplicity, we will analyze the case of a thin infinite strip of aspect ratio  $\nu = t/W \ll 1$ , that can rotate around its axis, which is perpendicular to  $\mathbf{H}$ . Let's assume that the strip was originally ZFC at an angle  $\Theta$  and  $H$  was subsequently applied (the initial condition in Fig. 2(a)). If  $H$  is high enough we can consider<sup>8</sup> that a current density of uniform modulus  $J_c(\Theta)$  flows over the whole volume.<sup>8</sup> This  $\mathbf{J}$  is parallel to the strip axis and it reverses sign at the plane that contains the axis and  $\mathbf{H}$ .

It has been shown<sup>9-11</sup> that, in this fully penetrated critical state and as long as  $\nu \tan \Theta \ll 1$ , the angle between  $\mathbf{M}_i$  and the sample normal  $\mathbf{n}$  is  $\alpha \sim \arctan(\frac{2}{3}\nu^2 \tan \Theta) \ll \Theta$ . That is,  $\mathbf{M}_i$  remains almost locked to  $\mathbf{n}$  due to a purely geometrical effect. For the particular crystal of the present study,  $\alpha$  should be smaller than  $1^\circ$  for  $\Theta \leq 80^\circ$ . Another result<sup>10</sup> is that, although in principle the geometrical factor relating  $M_i$  with  $J_c(\Theta)$  depends on  $\Theta$ , within that same angular range the variations are given by the factor  $(1 - \frac{2}{3}\nu^2 \tan^2 \Theta)$  and thus are negligible.

We now discuss what happens when the strip is ro-

tated away from this initial state by a small angle  $\delta\Theta$ . The result will depend on the direction of rotation. If  $\mathbf{n}$  approaches  $\mathbf{H}$  (this corresponds to the angular ranges  $90^\circ$  to  $180^\circ$  and  $270^\circ$  to  $360^\circ$  in Fig. 2(a)), the normal component  $H_\perp$  will increase, thus inducing screening currents at the edges of the crystal in the same direction as those already flowing. Vortices will then displace to satisfy the condition  $J \leq J_c(\Theta + \delta\Theta)$  everywhere. If  $J_c(\Theta + \delta\Theta) \leq J_c(\Theta)$  the new distribution will be analogous to the initial one, with  $J = J_c(\Theta + \delta\Theta)$  everywhere and the boundary of current reversal rotated by an angle  $\delta\Theta$  in order to remain parallel to  $\mathbf{H}$ . On the contrary, if  $J_c(\Theta + \delta\Theta) > J_c(\Theta)$ , the new field profile will propagate all the way to the center of the sample only if  $\delta H_\perp = H \sin(\Theta)\delta\Theta$ , is larger than the maximum possible additional screening  $\sim t[J_c(\Theta + \delta\Theta) - J_c(\Theta)]$ . The condition for the “full penetration of the rotational perturbation” is thus

$$H \sin(\Theta) \geq t \frac{dJ_c}{d\Theta} \quad (7)$$

If the inequality (7) is satisfied, the vortex system will evolve under rotations maintaining a fully penetrated critical state with uniform  $J$ . In other words, the state at any  $\Theta$  will be the same that would have formed by increasing  $H$  after ZFC at that orientation. Then, as long as  $\nu \tan \Theta \ll 1$ , the condition that  $\mathbf{M}_i$  is almost parallel to  $\mathbf{n}$  is preserved. We have experimentally confirmed this fact:  $\alpha \leq 1^\circ$  for all measurements conducted in this work, except in a very narrow angular range around the ab-planes, where a flip in  $\mathbf{M}_i$  occurs.<sup>10</sup> Thus, from now on we will plot all the results as a function of  $\Theta$ . Furthermore, we can obtain  $J_c(\Theta)$  by simply multiplying  $M_i$  by the angle independent factor that corresponds to the relation valid for  $\mathbf{H} \parallel \mathbf{n}$ . If eq. (7) is not satisfied,  $J$  will be subcritical in part of the sample and this relation is no longer valid.

If the crystal is rotated in such a way that  $\mathbf{n}$  moves away from  $\mathbf{H}$  (so  $H_\perp$  decreases), the new screening currents induced at the edges of the crystal will oppose to those already flowing. As the rotation progresses the boundary between the old and new  $\mathbf{J}$  directions will move inwards, until eventually the new critical state propagates to the whole sample. From that point the situation will again be analogous to that already discussed, except that  $\mathbf{M}_i$  will be paramagnetic instead of diamagnetic.

A rotation at fixed  $H$  is to some extent analogous to a hysteresis loop<sup>9</sup>. Rotating  $\mathbf{n}$  towards  $\mathbf{H}$  increases  $H_\perp$ , which is roughly equivalent to increasing  $H$  at  $\Theta = 0^\circ$ , moving along the lower (diamagnetic) branch of the loop. Decreasing  $H_\perp$  (either by rotating  $\mathbf{n}$  away from  $\mathbf{H}$  or by crossing the  $\mathbf{H} \parallel \mathbf{c}$  condition), is equivalent to reversing the field sweep, thus producing a switch to the other branch of the loop. This is a useful analogy for the analysis of the rotations, although it should not be pushed too far.

A basic difference is that a rotation also produces a variation in the parallel field component,  $\delta H_\parallel =$

$H \cos(\Theta) \delta\Theta$ . This generates screening currents flowing in opposite directions on the upper and lower surfaces of the strip, which produce a tilting force on the vortices.<sup>12–14</sup> If the perturbation propagates all the way to the central plane, the result is a rotation of the vortex direction following  $\mathbf{H}$ , the situation that we have implicitly assumed above. However, if pinning were strong enough it could preclude the propagation of the tilt beyond a certain depth, thus generating a critical state along the crystal thickness, with a central segment of the vortices remaining in the original direction.<sup>12–18</sup> If this effect were significant, as the rotation proceeded the orientation of the vortices would lag behind the field direction. In an extreme case, vortices deep inside the sample would rotate rigidly with it, a situation that has indeed been observed<sup>19–21</sup>. As we will show below, in the present case we have clear experimental evidence that the misorientation between the vortex direction and  $\mathbf{H}$  due to this lag effect is negligible, so all this complication can be ignored.

We now analyze the curves shown in Fig. 2. The measurement starts at  $\Theta \sim 30^\circ$  (point A) with  $\mathbf{n}$  rotating away from  $\mathbf{H}$ . Thus,  $\mathbf{J}$  initially undergoes a flip until the reversed fully penetrated critical state is formed (point B). From here the evolution of the system turns independent of the initial conditions and becomes two fold periodic. From point C ( $\Theta = 90^\circ$ ) to point E ( $\Theta = 180^\circ$ ) the system evolves in a fully penetrated critical state (in the hysteresis loop analogy, this is equivalent to increasing the field from zero to  $H$ ). Clearly visible within this angular range is the peak in both  $M_L$  and  $M_T$  at  $\Theta \sim 150^\circ$  (point D), that corresponds to the direction of the CD. At point E,  $M_T$  is null as expected by symmetry, while  $M_L$  begins a quick flip due to the reversal of the screening currents as  $H_\perp$  reaches a maximum at  $\mathbf{H} \parallel \mathbf{n}$  and then starts to decrease. The end of this flip at point G indicates that the critical state is completely reversed. From G to C' ( $\Theta = 270^\circ$ ) the evolution is analogous to a field decreasing portion of a loop.

Note that between E and G there is one unique angle (point F) where both  $M_L$  and  $M_T$  are null. This condition is equivalent to the unique  $H$  value in the switch from the lower to the upper branch of a  $M(H)$  loop where  $\mathbf{M}_i = \mathbf{0}$ . The fact that the condition  $M_L = 0$  occurs at the same angle where  $M_T = 0$  confirms that the background signal has been correctly subtracted, and we have systematically made use of this checking procedure.

In Fig. 2(a) the direction of rotation is such that the conditions  $\mathbf{H} \perp \mathbf{c}$ ;  $\mathbf{H} \parallel \text{CD}$  and  $\mathbf{H} \parallel \mathbf{c}$  proceed in that order. We define this as a clockwise (CW) rotation. In contrast, in a counter-clockwise (CCW) rotation the alignment occurs when  $\mathbf{n}$  is moving away from  $\mathbf{H}$ . The consequences of this difference are described below.

In Figure 2(b) the same CW data of Fig. 2(a) is shown in an  $M_L$  vs  $M_T$  polar graph (full symbols), together with the CCW rotation under the same conditions (open symbols). In both cases the initial behavior until the critical state is fully developed (portion A to B in the CW and P

to Q in the CCW) and the subsequent  $180^\circ$ -periodic evolution in the critical state (covering approximately two periods of  $180^\circ$ ) are clearly distinguished. Another feature that is apparent in this representation is that the magnetization vector passes through the origin ( $\mathbf{M}_i = \mathbf{0}$ ) and reaches the opposite quadrant each time that (i) a rotation starts moving  $\mathbf{n}$  away from  $\mathbf{H}$ ; or (ii) the  $\mathbf{n} \parallel \mathbf{H}$  condition is crossed.

Although the CW and CCW curves in Fig. 2(b) are similar (rotated in  $180^\circ$  with respect to each other) they also exhibit some differences. The most obvious one is that the peak at the CD direction (dotted line) is prominently seen in the CW rotation (point D), while in the CCW rotation it is partially suppressed by the flip of  $\mathbf{M}_i$ . The flip starts at  $\mathbf{H} \parallel \mathbf{n}$ , and ends at the angle  $\Theta_F$  where the fully reversed critical state is achieved. Making use of the loop analogy, this requires a field decrease of  $\sim 2H^*$ , where  $H^*(H, T)$  is the well known full penetration field, then

$$2H^* = H(1 - \cos \Theta_F) \quad (8)$$

This analysis indicates that there is a blind range in the rotation measurements, extending up to an angle  $\Theta_F$  from  $\mathbf{n}$ , where the critical state is not fully developed and thus  $J$  cannot be extracted. Depending on the direction of rotation, this blind range occurs either in the same quadrant of the CD (case CCW) or in the opposite (case CW). As  $\Theta_F$  decreases with  $H$ , in CCW rotations the peak due to the CD is totally hidden at low fields but can be fully measured at high enough  $H$ .

The values of  $\Theta_F$  are easily obtained from Figure 3(a), where  $M_i$  is plotted as a function of  $\Theta$  for the same two sets of data (CW and CCW) of Fig. 2(b). We observe here that the agreement between the CW and CCW data is excellent, thus they can complement each other to eliminate the blind region at low angles. Estimating  $\Theta_F \sim 25^\circ$  for the CW rotation and  $\Theta_F \sim 30^\circ$  for the CCW case, and using eq. (8) we obtain  $H^* \sim 370Oe$  and  $\sim 540Oe$  respectively. We can check the consistency of these estimates in two ways. First, we know that in a thin sample  $H^* \sim Jt$ . Combining with the critical state relation  $J \sim 60M_i/W$  (valid for a square platelet) we have  $H^* \sim 60M_it/W \sim 1.8M_i$ . From the figure we have  $M_i(\Theta_F) \sim 200G$  for the CW and  $\sim 340G$  for the CCW, so we get  $H^* \sim 360Oe$  and  $\sim 610Oe$  respectively, in very good agreement with the above estimates. On the other hand, we can compare the values of  $H^*$  obtained from eq. (8) with those directly measured in hysteresis loops at the appropriate angles. We have done so for several temperatures and fields, and we have systematically obtained very good consistency.

Fig. 3(a) confirms that the condition (7) is satisfied in this measurement. In fact, the largest slope  $dM_i/d\Theta \sim 1kG/rad$ , that occurs at  $\Theta \sim 33^\circ$ , implies that  $tdJ_c/d\Theta \sim 1.8kG/rad$ , which is indeed smaller than  $H \sin(\Theta) \sim 4.4kG$ . This condition is also fulfilled in all the cases discussed in the next section.

In order to compare the data measured by sample rotations with those resulting from traditional loop measurements, in Fig. 3(a) we also included  $M_i$  values at several  $\Theta$  obtained in the latter way at the same  $T$  and  $H$  (large open diamonds). The agreement is very good over the full range of angles, except that the loop values tend to be somewhat smaller. This is a feature observed for all measured fields, and can be explained by the fact that a rotation step is a process that takes only a couple of seconds, while a field increase and stabilization typically requires more than 1 minute in our magnetometer, during which the  $\mathbf{M}_i$  is already relaxing. Indeed, by performing short relaxation measurements we have verified that the rotation data approaches the loop data after 1-2 minutes. This results in another advantage of the rotations over the loops: measurements are made closer to the true initial critical state.

Finally, the coincidence of the CW and CCW rotations and the loops, particularly in the region of the peak due to the CD, rules out the possibility that vortices lag significantly behind the direction of  $\mathbf{H}$  in our rotating sample experiments. In summary, the information obtained from our rotation measurements is essentially the same as that provided by hysteresis loops, with several advantages including the possibility to acquire significantly more data points for each field. This feature permits a more detailed analysis of the peak associated with the uniaxial pinning of the CD, as will be shown in the next section.

#### IV. DETERMINATION OF THE LOCK-IN ANGLE

A complete set of rotations at 70K for different applied fields is shown in Figure 3(b). At high fields (above  $\sim 6kOe$ ) a well-defined peak at the CD direction is observed. At lower fields ( $1kOe \leq H \leq 5kOe$ ) the peak progressively broadens and transforms into a plateau (a certain angular range where  $M_i(\Theta) \sim const.$ ), while it shifts towards the c-axis. We had previously reported<sup>2</sup> all these features in  $YBa_2Cu_3O_7$  crystals.

The plateau represents the angular range of applied field over which it is energetically convenient for the vortices to remain locked into the columnar defects, thus its angular width is twice the lock-in angle  $\varphi_L$ . Below this angle, the vortices are subject to an invariant (and maximum) pinning force. According to theoretical models<sup>3,4</sup>

$$\varphi_L \simeq \frac{4\pi\sqrt{2\varepsilon_l\varepsilon_r(T)}}{\Phi_0 H} \quad (9)$$

where  $\varepsilon_l$  is the vortex line tension and  $\varepsilon_r(T)$  is the effective pinning energy.

Equation (9) predicts that  $\varphi_L$  should be inversely proportional to  $H$ . The improved resolution of the rotation measurements, that permits a much better determination

of the width of the plateau, allows us to test this dependence. To that end, we have measured several other sets of data similar to Figure 3(b), for a wide range of temperatures (35K to 85K). A few examples of the observed plateaus are shown in Figure 4.

We then extracted the plateau width for every measurement which displayed such a feature. This procedure was done very carefully, including an over-zealous estimate of the errors involved. The results for all measurable  $\varphi_L$  are plotted as a function of  $H^{-1}$  in Figure 5. This figure clearly demonstrates the  $H^{-1}$  dependence of  $\varphi_L$ , as evidenced by the solid lines which are the best linear fits to the data points for each temperature.

According to eq. (9), the data in fig. 5 should extrapolate to the origin, what is clearly not the case. For all the temperatures where reliable extrapolations can be made (35K to 80K) the linear fits systematically give a *positive* value of  $\varphi_L \sim 1.5^\circ$  to  $3^\circ$  at  $H^{-1} = 0$ , which is above the experimental error. There are at least two reasons for this discrepancy. In the first place, we experimentally determine  $\varphi_L$  from the intersection of straight lines extrapolated from the plateau and the slopes at both sides of it (see fig. 4). Due to the rounded ends of the plateau, this definition tends to *overestimate*  $\varphi_L$ . Second, the natural splay of the tracks will tend to wash away the expected cusp-like behavior at high fields, thus also contributing to the overestimate of  $\varphi_L$ . It is clear, on the other hand, that the influence of the splay is not too dramatic, as we indeed observe a rather sharp peak at high fields as seen in fig. 3(b). TRIM calculations show that<sup>22</sup>, in our irradiation conditions, the median radian angle of splay slowly increases from zero at the entry surface of the crystal to  $\sim 3^\circ$  at a depth of  $8\mu m$ , and then grows faster to  $\sim 6^\circ$  at the exit surface.

We now want to analyze whether eq. (9) provides a satisfactory description of the temperature dependence of the lock-in effect. As this expression does not account for the nonzero extrapolation of  $\varphi_L$  discussed in the previous paragraph, it would be incorrect to force a fit through the origin to determine the prefactor of  $H^{-1}$ . Instead, it is appropriate to identify such prefactor with the slopes  $\alpha(T) = d\varphi_L/d(H^{-1})$  of the linear fits. Indeed, the splay of the CD is a geometrical feature independent of  $H$  and hence it should only add a constant width to the plateau, without changing its field dependence. To a first approximation, the rounded edges of the plateau will also introduce an additive constant, without significantly affecting the slope. Figure 6 shows the temperature dependence of  $\alpha(T)$  (solid symbols). As expected,  $\alpha(T)$  decreases with increasing  $T$ , reflecting the fact that the lock-in angle at fixed  $H$  decreases with  $T$  due to the reduction of both the line tension and the pinning energy. For a quantitative analysis it is necessary to know the expressions for  $\varepsilon_l$  and  $\varepsilon_r(T)$ . In our experiments the appropriate line tension is that corresponding to in-plane deformations (see pages 1163-1164 in Ref.<sup>4</sup>),  $\varepsilon_l = (\varepsilon^2\varepsilon_0/\varepsilon(\Theta)) \ln \kappa$ , where  $\varepsilon_0 = (\Phi_0/4\pi\lambda)^2$ ,

the penetration depth  $\lambda$  corresponds to  $\mathbf{H} \parallel \mathbf{c}$ , the mass anisotropy  $\varepsilon \ll 1$  and  $\varepsilon^2(\Theta) = \cos^2(\Theta) + \varepsilon^2 \sin^2(\Theta)$ . The temperature dependence of the superconducting parameters appears in  $\varepsilon_l$  through  $\lambda(T)$ . On the other hand,  $\varepsilon_r(T)$  is given by<sup>4,3</sup>

$$\varepsilon_r(T) = \eta \frac{\varepsilon_0}{2} \ln \left( 1 + \frac{r^2}{2\xi^2} \right) \times f(x) \quad (10)$$

where  $r \approx 50\text{\AA}$  is the radius of the tracks,  $\xi$  is the superconducting coherence length, and the dimensionless *efficiency factor*  $\eta \leq 1$  accounts for the experimental fact that the pinning produced by the CD is smaller than the ideal.<sup>23</sup> Besides the intrinsic temperature dependence of the superconducting parameters, this expression contains an additional temperature dependent factor  $f(x)$ , known as the *entropic smearing* function, which accounts for the thermal fluctuations of the flux lines. Here  $x = T/T_{dp}$ , where  $T_{dp}$  is a characteristic field-independent *depinning temperature*. Combining all these elements, at the track's direction  $\Theta = \Theta_{CD}$  we obtain

$$\alpha(T) \approx \frac{\Phi_0 \varepsilon}{8\pi \lambda^2} \ln \left( 1 + \frac{r^2}{2\xi^2} \right) \times \left[ \eta \frac{2 \ln \kappa}{\varepsilon(\Theta_D)} f(x) \right]^{1/2}, \quad (11)$$

In the original work of Nelson and Vinokur<sup>3</sup>, where only a *short range* pinning potential was considered, the entropic function for  $x > 1$  was approximately given by  $f_{sr}(x) \sim x^2 \exp(-2x^2)$ . However, according to a further refinement of the model<sup>4</sup>, where the *long range* nature of the pinning potential was taken into account, this function (for  $x > 1$ ) takes the form  $f_{lr}(x) \sim \exp(-x)$ .

We can now fit the experimentally determined  $\alpha(T)$  using eq. (11). To that end we use the long range result  $f_{lr}(x)$  and fix the reasonably well known superconducting parameters of the material  $\varepsilon \approx 1/5$ ;  $\ln \kappa \approx 4$  and  $\xi = 15\text{\AA}/\sqrt{1-t}$  (where  $t = T/T_c$ ). We also assume the usual two-fluid temperature dependence  $\lambda(T) = \lambda_L/2\sqrt{1-t^4}$ , where  $\lambda_L$  is the zero-temperature London penetration depth. The free parameters are then  $T_{dp}$  and the combination  $\lambda_L/\eta^{1/4}$ . The best fit, shown in figure 6 as a solid line, yields  $\lambda_L/\eta^{1/4} = 360\text{\AA}$  and  $T_{dp} = 30\text{K}$ .

Based on the results of figs. 5 and 6, there are a number of considerations that can be made at this point. The first one is that the Bose-glass scenario contained in eqs. (9) to (11) provides a quite satisfactory description of the lock-in effect over the whole range of temperature and field of our study. In addition, the obtained  $T_{dp}$  is smaller, but still reasonably similar to the value  $\sim 41\text{K}$  that we had previously found for several YBCO crystals using a completely different experimental method.<sup>23,24</sup> This low  $T_{dp}$  (well below the initial theoretical expectations) indicates that the efficiency factor  $\eta$  is rather small, what is also consistent with the less than optimum  $J_c$  observed here and in several previous studies. For low matching fields as that used in the present work, it was estimated<sup>23</sup> that  $\eta \sim 0.2 - 0.25$ .

The exact value of  $\eta$  has little influence in our estimate of  $\lambda_L$ , as it only appears as  $\eta^{1/4}$ . For  $\eta = 0.2$  and  $\eta = 1$  we get  $\lambda_L = 250\text{\AA}$  and  $360\text{\AA}$  respectively, a factor of 4 to 5 smaller than the accepted value  $\lambda_L \sim 1400\text{\AA}$ . Zhukov et al.<sup>25</sup> had reported a similar discrepancy when studying the lock-in effect by both CD and twin boundaries in YBCO. In a previous study in YBCO crystals with CD, we had also found that the misalignment between  $\mathbf{B}$  and  $\mathbf{H}$  at low fields (due to anisotropy effects) was well described using a  $\lambda_L$  significantly smaller than the accepted value<sup>2</sup>. Thus, this numerical discrepancy appears to be a common result associated to the study of angular dependencies in YBCO-type superconductors with correlated disorder.

Finally, it is relevant to note that eq. (9) was derived for the *single vortex pinning* regime, which occurs below a temperature dependent accommodation field<sup>4,23</sup>  $B^*(T) < B_\Phi$ , while a large fraction of the data shown in fig. 5 lies above this line, in the *collective pinning* regime. Unfortunately, to our knowledge there is no available expression for  $\varphi_L(H, T)$  in the collective regime. Blatter et al.<sup>4</sup> only argued that collective effects should result in a reduction of the lock-in angle. The experimental fact is that eq. (9) satisfactorily describes both the temperature and field dependence of  $\varphi_L$ . This suggests that, at least to a first approximation, collective effects in the range of our measurements simply result in a different prefactor in eq. (9). Clearly, lock-in effects in the collective regime deserve further theoretical study.

## V. CONCLUSIONS

We have measured the irreversible magnetization ( $\mathbf{M}_i$ ) of an  $\text{ErBa}_2\text{Cu}_3\text{O}_{7-\delta}$  single crystal with columnar defects (CD), using an alternative technique based on sample rotation under a fixed magnetic field. The resulting  $\mathbf{M}_i(\Theta)$  curves for several temperatures agreed very well with independent hysteresis loop experiments, showing a peak in the CD direction at higher fields, while a very well defined plateau due to the lock-in of the vortices into the CD was observed at lower fields. The lock-in angle satisfactorily follows the field and temperature dependence predicted by the Bose-glass scenario.

## VI. ACKNOWLEDGMENTS

Work partially supported by FAPESP, Brazil, Procs. #96/01052-7 and #96/05800-8; ANPCyT, Argentina, PICT 97 No.01120; and CONICET PIP 4207.

- <sup>1</sup> L. Civale, A. D. Marwick, T. K. Worthington, M. A. Kirk, J. R. Thompson, L. Krusin-Elbaum, Y. Sun, J. R. Clem, F. Holtzberg, *Phys. Rev. Lett.* **67**, 648 (1991).
- <sup>2</sup> A. Silhanek, L. Civale, S. Candia, G. Nieva, G. Pasquini, H. Lanza, *Phys. Rev. B* **59**, 13620 (1999).
- <sup>3</sup> D. R. Nelson and V. M. Vinokur, *Phys. Rev. Lett.* **68**, 2398 (1992); *Phys. Rev. B* **48**, 13060 (1993).
- <sup>4</sup> G. Blatter, M. V. Feigel'man, V. B. Geshkenbein, A. I. Larkin, V. M. Vinokur, *Rev. Mod. Phys.* **66**, 1125 (1994).
- <sup>5</sup> A. Silhanek, D. Niebieskikwiat, L. Civale, M. A. Avila, O. Billoni and D. Casa, *Phys. Rev. B* **60**, 13189 (1999).
- <sup>6</sup> M. A. Avila, *Ph. D. Thesis*, University of Campinas (UNICAMP), Brazil (2001).
- <sup>7</sup> S. Candia and L. Civale, *Supercond. Sci. Technol.* **12**, 192 (1999).
- <sup>8</sup> J. R. Clem and A. Sanchez, *Phys. Rev. B* **50**, 9355 (1994).
- <sup>9</sup> R. Prozorov, A. Poddar, E. Sheriff, A. Shaulov, Y. Yeshurun, *Physica C* **264**, 27 (1996).
- <sup>10</sup> A. A. Zhukov, G. K. Perkins, Yu. V. Bugoslavsky, A. D. Caplin, *Phys. Rev. B* **56**, 2809 (1997).
- <sup>11</sup> S. K. Hasanain, I. Ahmad and R. Semerad, *Supercond. Sci. Technol.* **12**, 633 (1999).
- <sup>12</sup> J. R. Clem, *Phys. Rev. B* **26**, 2463 (1982).
- <sup>13</sup> J. R. Clem and A. Perez-Gonzalez, *Phys. Rev. B* **33**, 1601 (1986).
- <sup>14</sup> A. Perez-Gonzalez and J. R. Clem, *Phys. Rev. B* **42**, 4100 (1990).
- <sup>15</sup> H. P. Goeckner and J. S. Kouvel, *Phys. Rev. B* **50**, 3435 (1994).
- <sup>16</sup> S. K. Hasanain, Sadia Manzoor, M. Aftab, *Physica C* **272**, 43 (1996).
- <sup>17</sup> M. K. Hasan and J. S. Kouvel, *Physica C* **276**, 289 (1997).
- <sup>18</sup> I. M. Obaidat, H. P. Goeckner and J. S. Kouvel, *Physica C* **291**, 8 (1997).
- <sup>19</sup> V. K. Vlasko-Vlasov, U. Welp, G. W. Crabtree, D. Gunter, V. V. Kabanov, V. I. Nikitenko, L. M. Paulius, *Phys. Rev. B* **58**, 3446 (1998).
- <sup>20</sup> I. M. Obaidat, S. J. Park and J. S. Kouvel, *Physica C* **308**, 185 (1998).
- <sup>21</sup> M. K. Hasan, J. Shobaki, I. A. Al-Omari, B. A. Albiss, M. A. Al-Akhras, K. A. Azez, A. K. El-Qisari, J. S. Kouvel, *Supercond. Sci. Tech.* **12**, 606 (1999).
- <sup>22</sup> D. Niebieskikwiat, A. Silhanek, Civale, G. Nieva, P. Levy and L. Krusin Elbaum *Phys. Rev. B*, **63**, 144504 (2001).
- <sup>23</sup> L. Krusin-Elbaum, L. Civale, J. R. Thompson and C. Feild, *Phys. Rev. B* **53**, 11744 (1996).
- <sup>24</sup> L. Civale, G. Pasquini, P. Levy, G. Nieva, D. Casa and H. Lanza, *Physica C* **263**, 389-395 (1996).
- <sup>25</sup> A. A. Zhukov, G. K. Perkins, J. V. Thomas, A. D. Caplin, H. Kupfer, and T. Wolf, *Phys. Rev. B* **56**, 3481 (1997).

Figure 1.  $M_T$  versus  $M_L$  polar graph in the Meissner phase for  $T = 60K$  and  $H = 50Oe$ . Open symbols: raw data. Solid symbols: pure Meissner response (the remnant contribution was removed).

Figure 2. (a) Components of the magnetization vector,  $M_T$  and  $M_L$ , as a function of the angle for  $T = 70K$  and  $H = 8kOe$ . The direction of rotation is such that the conditions  $\mathbf{H} \perp \mathbf{c}$ ;  $\mathbf{H} \parallel \mathbf{CD}$  and  $\mathbf{H} \parallel \mathbf{c}$  proceed in that order. (b)  $M_T$  vs  $M_L$  polar graph of the same CW rotation of (a) (full symbols) together with the CCW rotation.

Figure 3. Irreversible magnetization  $M_i$  as a function of  $\Theta$  at  $T = 70K$  for (a)  $H = 8kOe$  together with data obtained from hysteresis loop measurements (b) several fields.

Figure 4. Irreversible magnetization  $M_i$  as a function of  $\Theta$  in the region of the plateau at  $T = 50K$  and  $70K$  for several fields.

Figure 5. Lock-in angle  $\varphi_L$  versus  $1/H$  for several temperatures. The straight lines are fits according to equation (9).

Figure 6. Temperature dependence of the slopes  $\alpha(T) = d\varphi_L/d(H^{-1})$  of the linear fits of fig. 5 (full symbols). The solid line is a fit to eq. (11).

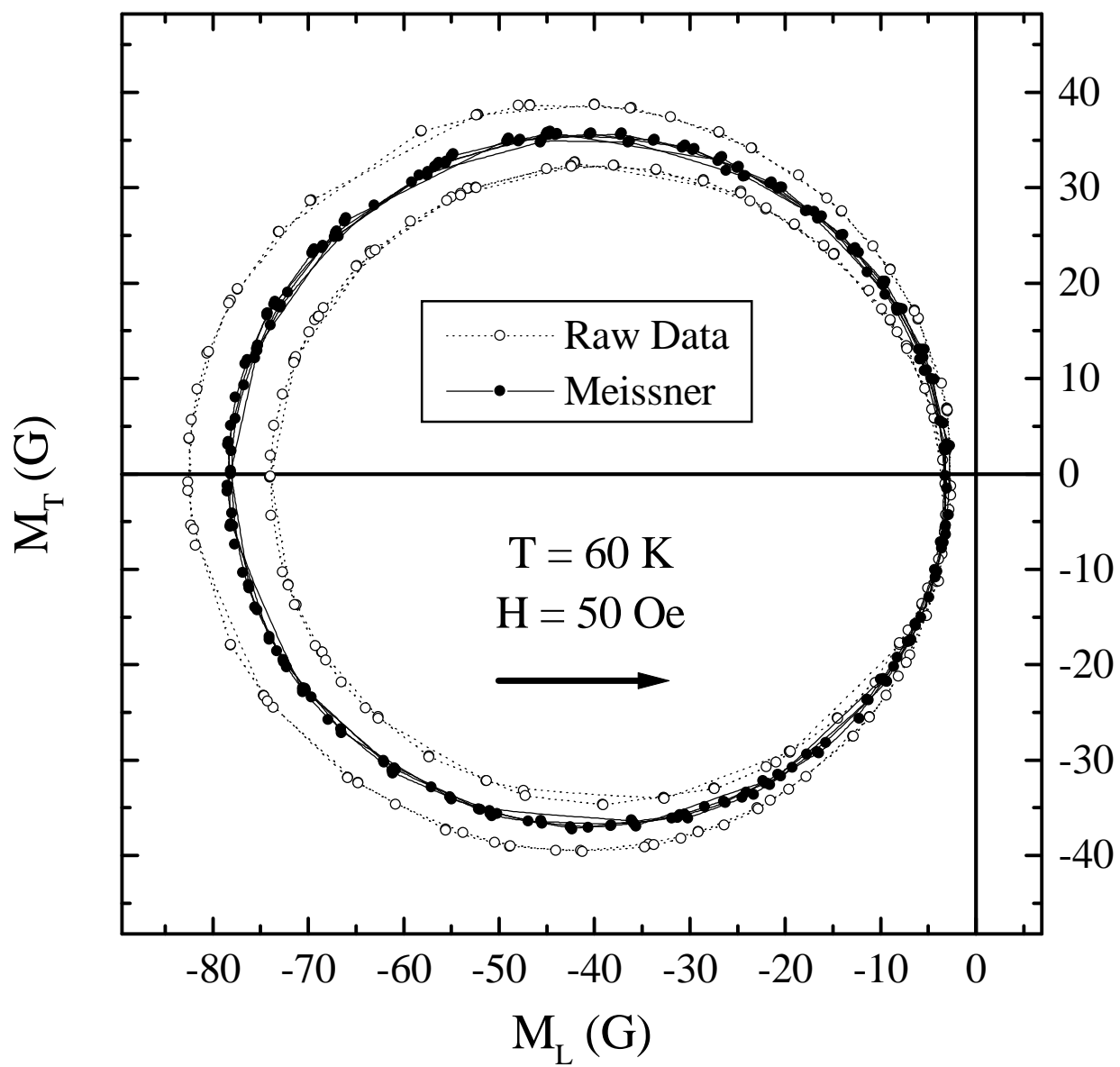
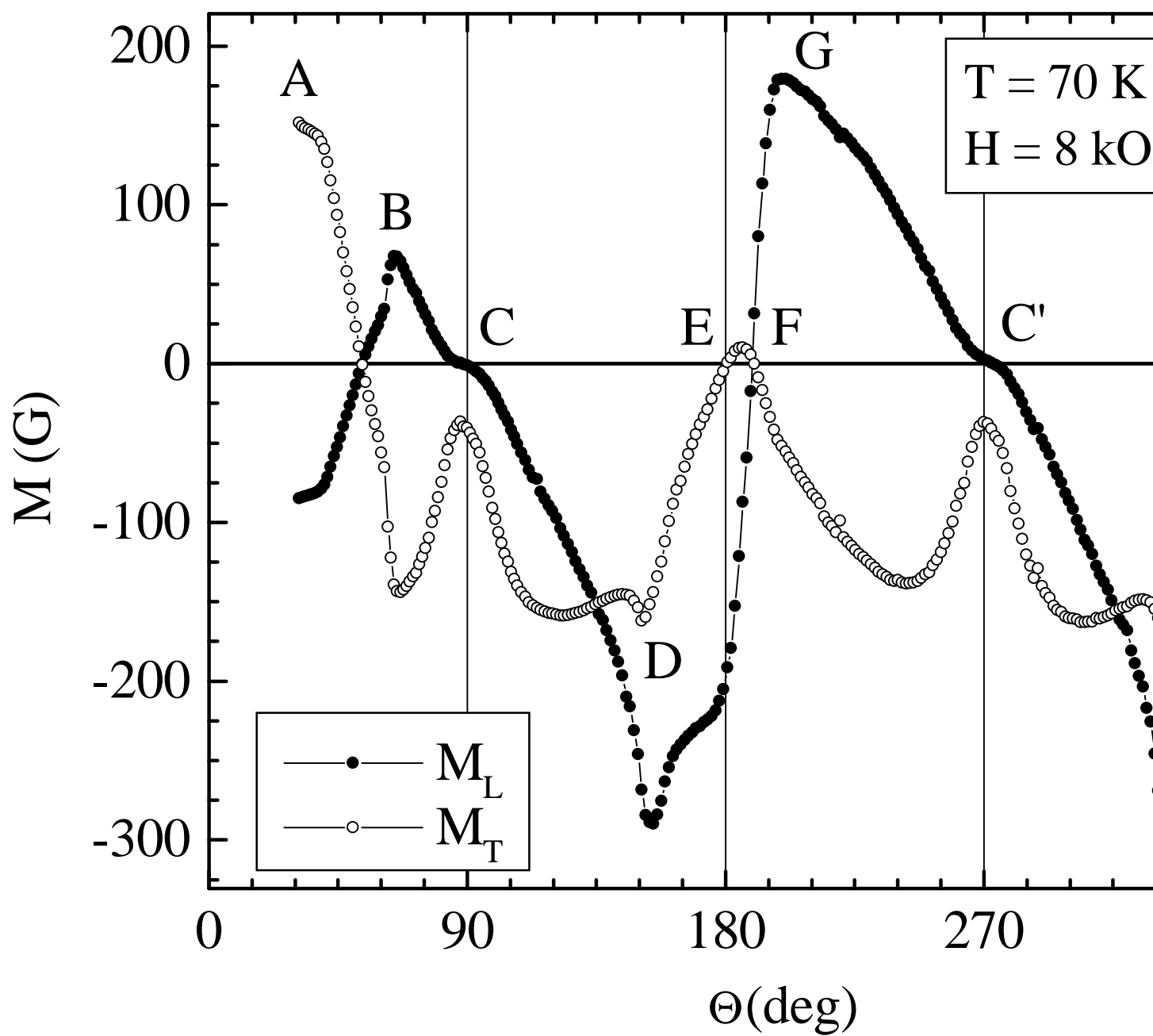


Figure 1





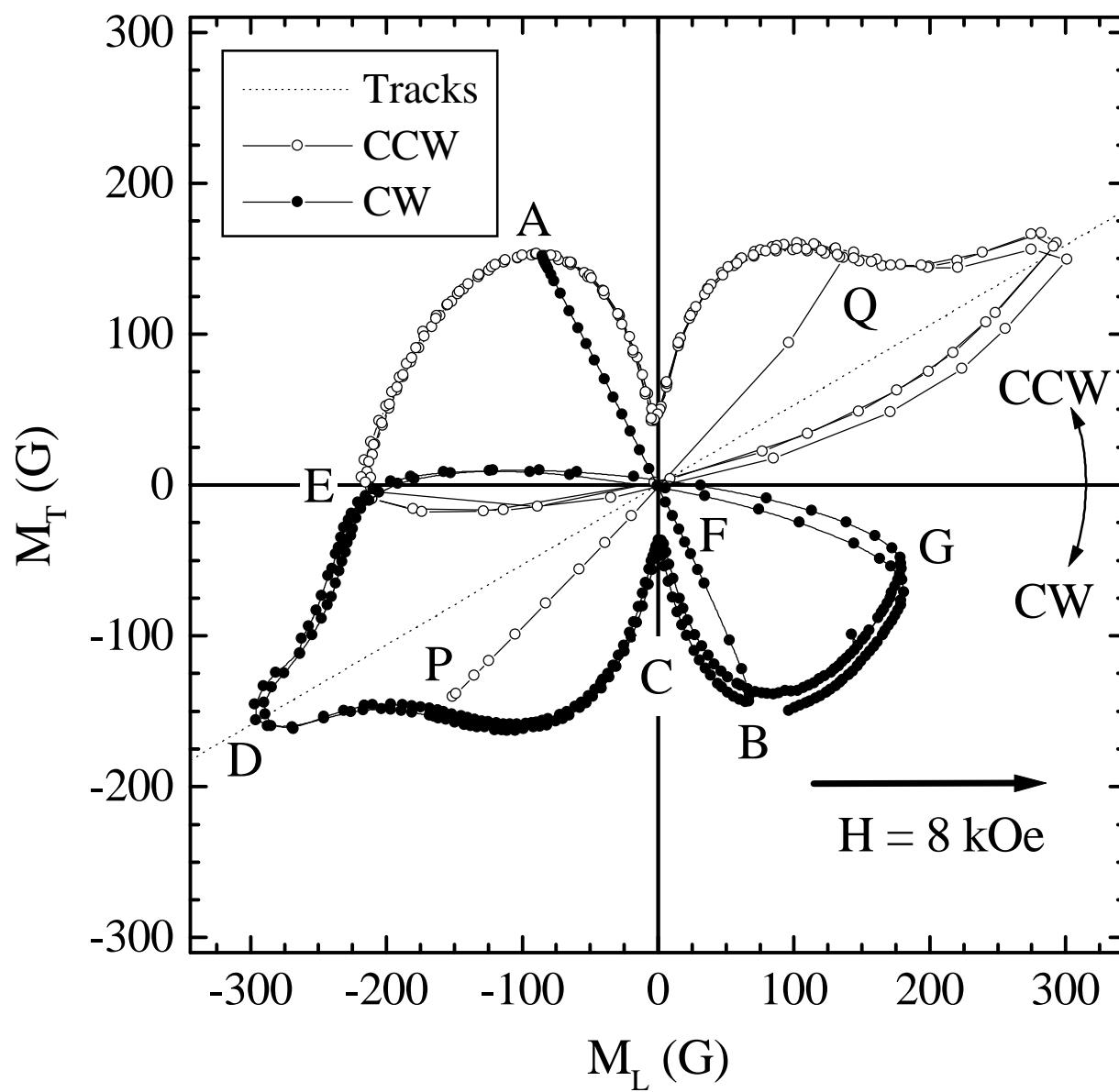


Figure 2(b)

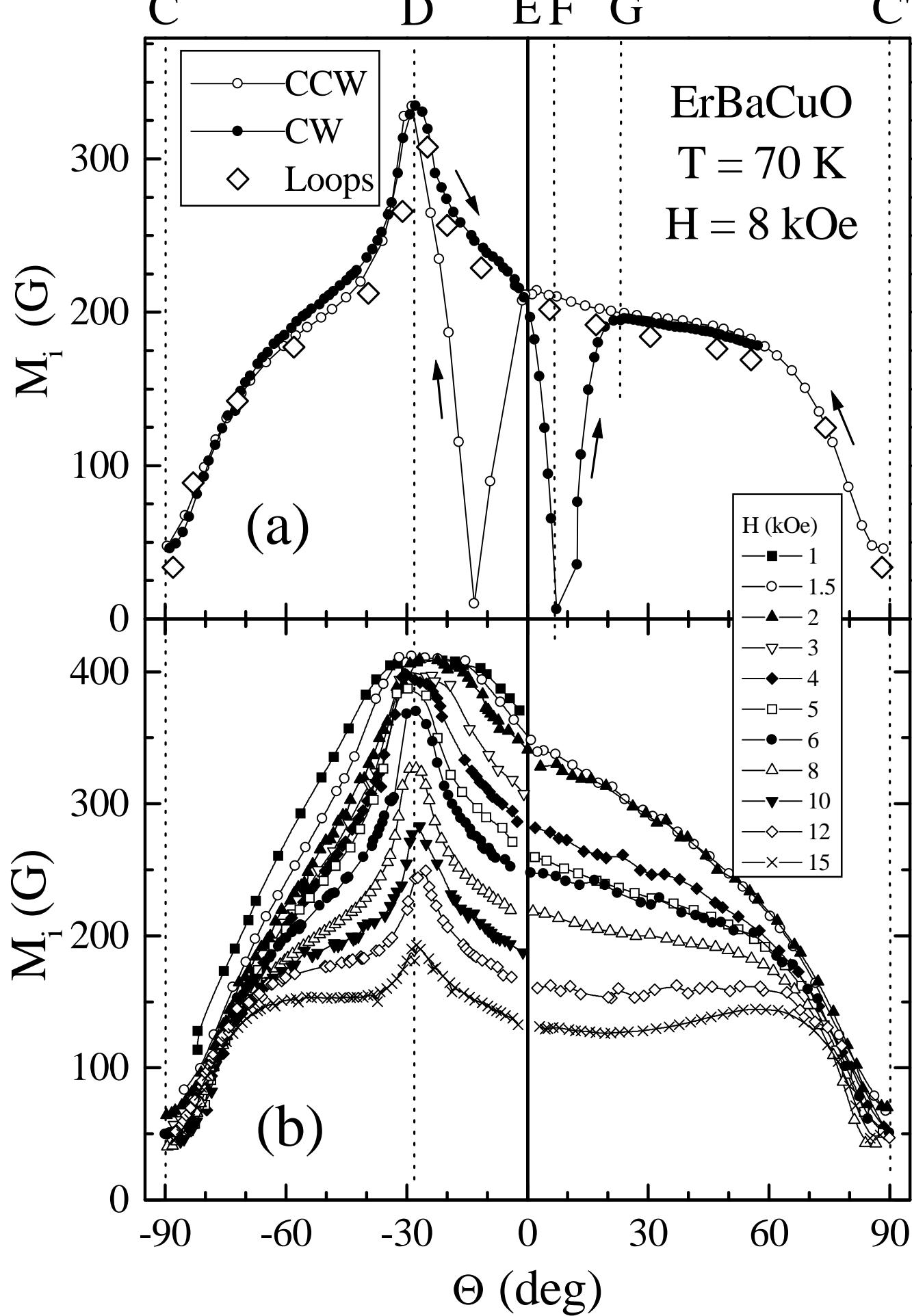


Figure 3

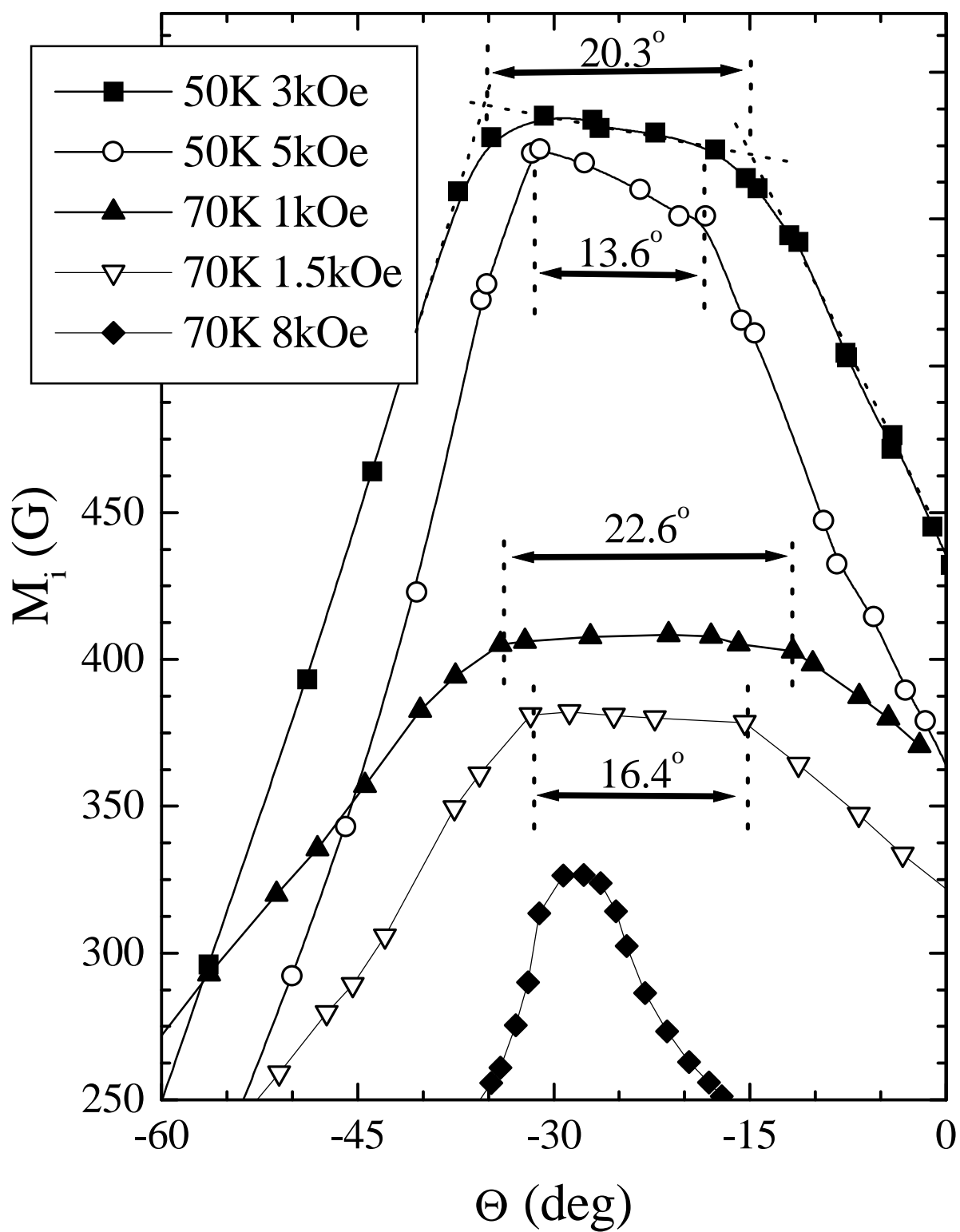


Figure 4

